JOINT EUROPEAN TORUS

JET–P(90)50

L-G. Eriksson, T. Hellsten
and JET Team

Calculations of ICRF Driven Current Profiles Caused by TTMP and ELD

Calculations of ICRF Driven Current Profiles Caused by TTMP and ELD

L-G. Eriksson, T. Hellsten[1]
and JET Team*

JET-Joint Undertaking, Culham Science Centre, OX14 3DB, Abingdon, UK

[1]Royal Institute of Technology, Stockholm, Sweden
** See Appendix 1*

Preprint of an Paper presented at the Joint Varenna-Lausanne International Workshop:
Theory of Fusion Plasmas, Varenna, 27th-31st August 1990

CALCULATIONS OF ICRF DRIVEN CURRENT PROFILES CAUSED BY TTMP AND ELD.

L-G. Eriksson* and T. Hellsten

*JET-Joint Undertaking, Abingdon, Oxon, OX14 3EA, U.K.
Royal Institute of Technology, S-100 44 Stockholm, SWEDEN

A model for current drive by electron Landau damping and transit time magnetic pumping in the ICRF-regime has been introduced in the global wave code LION [1] to calculate global current drive efficiency and current profiles. The frequency regime near the fourth harmonic of the deuterium cyclotron frequency is a suitable regime for demonstrating current drive in JET. Trapped particle effects are found to be a severe limitation for this low frequency regime. They give rise to an even more strongly peaked current profile than the power deposition profile.

1. Introduction

Non-inductive current drive is essential for achieving a continuous operating fusion reactor based on the tokamak principle. Current generation by neutral beams and waves in the radio frequency regime have been proposed [1-3] and tested experimentally [4-5]. Among the suggested method is current drive based on electron damping of the fast magnetosonic wave in the ion cyclotron frequency range. An advantage with this method compared to lower hybrid current drive is that accessibility of the waves to the centre of the plasma is easier to obtain [6-8]. ICRH is a well proved method in large tokamaks. It is therefore of interest to investigate its potential for current drive. Direct damping of the magnetosonic wave by electron Landau damping (ELD) and transit time magnetic pumping (TTMP) have already been demonstrated [9-10]. However, any measurable current drive has not yet been achieved.

Electron damping of the fast magnetosonic wave is usually weak because the parallel electric field and the gyro radii of the electrons are small. To make things worse, the two forces giving rise to ELD and TTMP are for the magnetosonic wave directed opposite to each other and of comparable magnitude so that the two accelerating forces nearly cancel each other. Thus in order to obtain sufficiently strong damping it is necessary to have a large fraction of the total electron population in resonance with the wave. This can only be achieved if the phase velocity is close to the thermal velocity of the electrons. Originally this was thought to be an advantage since accelerating particles with low parallel velocities is energetically more effective [2]. However, this has evident drawbacks not only are the electrons relatively rapidly isotropized by collisions but a large fraction of the electrons are trapped in the toroidal magnetic field and will therefore not carry any current [11].

It is an advantage to have strong ELD and TTMP damping since other damping mechanisms exist e.g. ion cyclotron damping at the fundamental resonance and its harmonics, linear mode conversion at the Alfvén wave resonance, or at the perpendicular ion cyclotron resonance, and non-linear mode conversion into ion-Bernstein waves and quasi-modes [12]. For current drive by ELD and TTMP these absorption mechanisms will then appear as parasitic reducing the overall efficiency. To calculate the total efficiency and the driven current profiles, the global wave propagation problem has to be solved. When the wave field is known one can then evaluate the local absorption by ELD and TTMP and the driven current. In this report we have used a modified version of the LION-code to calculate the wave field and a model developed by Chiu *et al.* [8] to calculate the local current drive efficiency. In the latter model the distortion of the electron velocity distribution is assumed to be small so that the contribution from the RF-operator coming from the distortion can be neglected. By using a model operator for the collisions instead of the proper Coulomb collision operator the current drive efficiency can then be expressed in terms of quadratures. The model operator used includes pitch angle scattering by ions and electrons but no energy diffusion. Drag is included by a calibration function. The operator is chosen so that the total electron momentum is conserved for electron-electron collisions.

2. Current Drive Model

The wave field in a tokamak equilibrium is calculated with the LION-code [13]. Originally the electron damping was introduced into the LION-code by using the local dispersion relation for the magnetosonic wave to express the total damping in terms of the $E\lambda$-field component [14], where λ is the direction perpendicular to the magnetic field

and parallel to the magnetic surface. The damping can then be calculated by adding a correction $\epsilon_{\lambda\lambda}$ to the $\epsilon_{\lambda\lambda}$-term in the dielectric tensor [15]

$$\epsilon_{\lambda\lambda} = i \frac{\sqrt{\pi}\ \omega\, \omega_{pe}^2\ R\, k_\perp^2\ v_{the}}{2\ c^2\ n_\phi\, \omega_{ce}^2} \exp\left(- \left(\frac{\omega R}{n_\phi v_{the}} \right)^2 \right) \qquad (1)$$

here ω, ω_{pe} and ω_{ce} denote the wave frequency, the electron plasma frequency and the electron gyro frequency, respectively, n_ϕ is the toroidal wave number, $k_\perp$ the perpendicular wave number, R the plasma radius, c velocity of light and v_{the} the thermal electron velocity defined as $v_{the} = \sqrt{2kT_e/m_e}$. This approximation was obtained under the assumption $/ \epsilon_{zy}\, \omega^2 / c^2 / >> k_x\, k_y$. If we instead keep the terms neglected by this assumption we can write the correction terms as

$$\epsilon_{\lambda\lambda} = \epsilon_{\lambda\lambda}(1 + \delta) \qquad (2)$$

where $\delta = C_R^2 + C_I^2$

$$C_R = \frac{2\, c^2\ \omega_{ce}\ \epsilon_{xy}\ R_e\ (\epsilon_{zz})}{v_{the}\ \omega / \epsilon_{zz} /^2 / \frac{\epsilon_{xx}\omega^2}{c^2} - k_z^2 /}$$

$$C_I = \frac{2\, c^2\ \omega_{ce}\ \epsilon_{xy}\ I_m\ (\epsilon_{zz})}{v_{the}\, \omega / \epsilon_{zz} /^2 / \frac{\epsilon_{xx}\omega^2}{c^2} - k_z^2 /}$$

The coordinates (x, y, z) form a local coordinate system so that z is parallel to the magnetic field.

For calculating the current drive efficiency when the local electron absorption is known we use the method by Chiu *et al.* [8]. The local current drive efficiency becomes

$$\frac{j}{p} = \left(\frac{e}{m_e v_0 v_{the}} \right) \frac{\int_{X_R}^{\infty} dx\, f(X_R, Z_{eff})\ L\ \Psi_R /_{\xi=\xi_R}\ e^{-x} A(x)}{\int_{X_R}^{\infty} dx\ e^{-x} A(x)} \qquad (3)$$

where $L = \frac{v_{the}^2}{2 v_{//}} \frac{\partial}{\partial v_{//}} = \frac{\partial}{\partial x} - \frac{\xi}{x} \frac{\partial}{\partial \xi}$

$$v_0 = \frac{4\pi\, n_e\, e^4\, \ell n \Lambda}{m_e^2\, v_{the}^3}$$

Ψ_R and f are given in Ref. [8]. A few errors appeared in this article. I and K_1 should be

$$I = \frac{4}{3} \int_0^{Bmin/Bmax} \frac{\pi \xi d\xi}{2E(k^2)\sqrt{1-\xi}} \qquad (4)$$

and

$$K_1 = \int_0^{\infty} x^{3/2} e^{-x} \left(\eta + \eta' - \frac{\eta}{2x}\right) \Phi(x) dx \qquad (5)$$

3. Current Drive Efficiency and Current Drive Profiles

Since the normalization constant in front of Eq. (3) is proportional to T_e/n_e a high electron temperature and a low density is an advantage for a high efficiency. However, the temperature does not only enter through the normalization constant but appears also implicitly in the other terms. For instance, if the phase velocity is kept constant, which is a typical experimental condition, the number of trapped resonant particles increases with temperature. This may sometimes reduce the efficiency as can be seen in Fig. 1, where we plotted the current drive efficiency versus toroidal mode numbers for different conditions with ϵ=0.03.

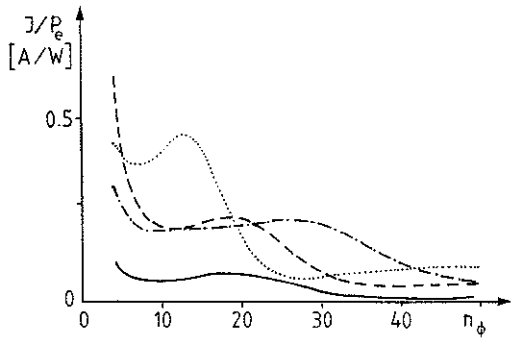

Fig. 1 Current drive efficiency versus n_ϕ R_0 = 3.09m.
-------f = 33MHz $n_e = 3 \cdot 10^{19} m^{-3}$, B_0 = 3.4T, T = 7keV
·····f = 33MHz $n_e = 3 \cdot 10^{19} m^{-3}$, B_0 = 3.4T, T = 15keV
———f = 33MHz $n_e = 1 \cdot 10^{20} m^{-3}$, B_0 = 3.4T, T = 7keV
—·—·—f = 48MHz $n_e = 3 \cdot 10^{19} m^{-3}$, B_0 = 1.4T, T = 7keV

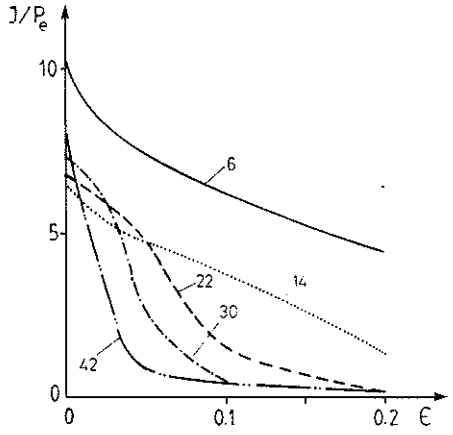

Fig. 2 Current drive efficiency versus inverse aspect ratio ϵ for θ= 0
The numbers indicate toroidal mode number.

In absence of trapped particle effects the efficiency is lowest for $n_\phi \approx 14$, for the parameters: f = 48MHz $n_e = 3 \cdot 10^{19} m^{-3}$, B_0 = 1.4T and T = 7keV used in Fig. 2. For low toroidal mode numbers the phase velocity becomes high resulting in a low Coulomb collision frequency and a high efficiency. For large toroidal mode numbers the phase

velocity becomes small and the wave interacts then with electrons with low parallel velocity for which it is energetically more effective to increase their momentum [1]. However, the latter effects are only effective near the magnetic axis where trapped particle effect is less important. For larger inverse aspect ratio, ϵ, the efficiency reduces significantly as originally suggested by Bickerton [11].

For outboard location of the antennae, like in the JET-machine, the wave interacts at the first transit at a poloidal angle $\theta = O$ for which the trapping is at is maximum. For weak absorption the wave field fills up the whole plasma and the absorption occurs at all poloidal angles. For $\theta = \pi$ the trapped particle effect is at is minimum. The variations of the efficiency versus poloidal angle χ, as definite in Ref. [13], can be seen in Fig. 3 for $n_\phi = 30$. For large ϵ the variation of $k_{//}$ along the magnetic surface becomes so large that the efficiency decreases with χ.

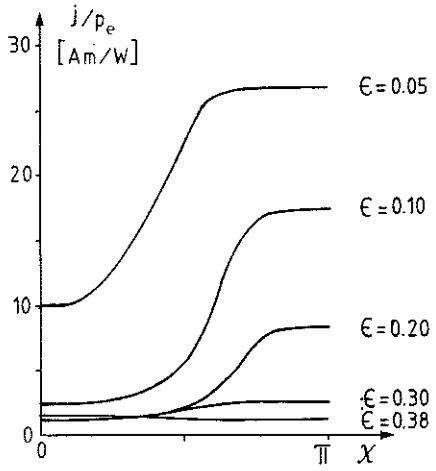

Fig. 3 Current drive efficiency versus poloidal angle χ. The parameters are the same as used in Fig. 6 except $n_e(o) = 3 \cdot 10^{19} m^{-3}$.

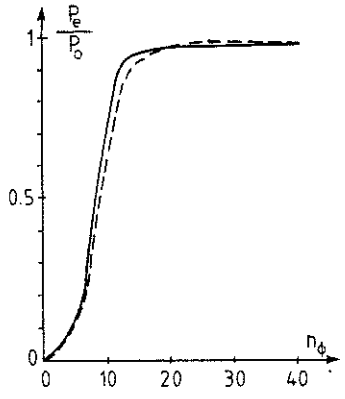

Fig. 4 Fraction of power absorbed by TTMP/ELD versus n_ϕ.

To increase the efficiency by increasing T_e/n_e at fixed ratio between phase velocity and thermal velocity is not always feasible. When optimising the current drive efficiency one can not only optimize the current per watt absorbed by TTMP/ELD but one has also to take into account the power absorbed by other absorption mechanisms which may not contribute to any current drive. To do so one has to avoid scenarii with strong ion cyclotron damping. There are in principle three regimes one can choose. Either to work at a high multiple of the cyclotron frequency for which the cyclotron damping becomes weak, or to work below the fundamental ion cyclotron frequency, or finally to work at the fundamental cyclotron frequency with a large concentration of resonant ions. The first frequency range has the disadvantage that absorption by α-particles is still strong for higher multiples of the cyclotron frequency. The last two regimes have the

disadvantage of the presence of the Alfvén wave resonance at the plasma boundary on the inboard side. A suitable scenario to demonstrate current drive in JET is the frequency regime close to the fourth harmonic of D.

To compare the efficiency for various condition we choose two different equilibrium profiles: One with a strongly peaked density profile as obtained with pellet injection

$$n_e = 3.04 \cdot 10^{19} (1-s^2)^{0.2} + 6.0 \cdot 10^{19} \exp (-7.67\ s^2) m^{-3}$$

$$T = 12 \exp (-7\ s^2) keV$$

The other profile is one with rather low density with a flat profile and high electron temperature

$$n_e = 2.0 \cdot 10^{19} (1-0.99\ s^2)^{0.55} m^{-3}$$

$$T = 12.0 (1-0.99 s^2)^2 keV$$

where s labels the flux surfaces $s = \sqrt{\Psi/\Psi_0}$. Both have the parameters $B_0 = 1.4T$ *and* $f = 48$ *MHz*. Here we have assumed electron and ion temperatures to be equal. Since a small amount of hydrogen is usually unavoidable we have assumed hydrogen to be the only impurity with the ratio $n_H/n_D = 0.05$.

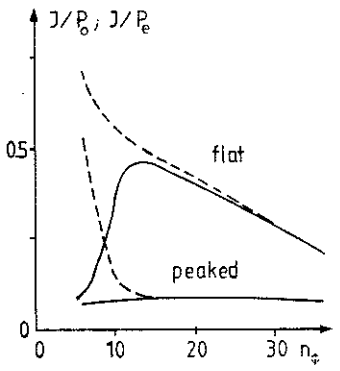

Fig. 5 Global current drive efficiency versus n_ϕ. Full lines J/P_o and dashed lines J/P_e.

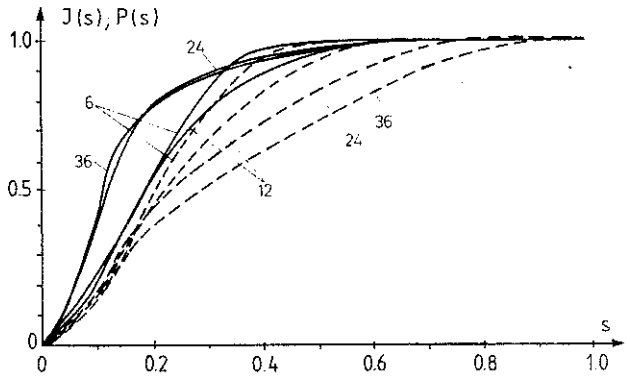

Fig. 6. Full lines $J(s)$ and dashed lines $P(s)$. The numbers indicate toroidal mode numbers. P and J are normalized to 1 at $s = 1$.

For $n_\phi > 12$ more than 90% of the power is absorbed by TTMP/ELD see Fig. 4. The remaining power is absorbed as cyclotron absorption at the second harmonic for hydrogen or 3th, 4th and 5th harmonics for deuterium. Hydrogen absorption dominates for these parameters over deuterium absorptions.

In Fig. 5 we compare the total efficiency, J/P_o for the two scenarii. A maximum of 0.45 A/W is obtained. The total current drive efficiency decreases rapidly for low toroidal mode numbers mainly because of a smaller fraction of the total power is absorbed by TTMP/ELD. The equilibrium corresponding to pellet injection has a lower efficiency. This is due to the higher density.The trapped particle effects give rise to even more peaked driven current profiles than the power deposition profiles. In Fig. 6 we have compared

$$J(s) = \int_{V(s)} j\, dV \quad \text{and} \quad P_e(s) = \int_{V(s)} p_e\, dV$$

for different toroidal mode numbers for the flat profile. The higher toroidal mode numbers show a broader power deposition profile but a more narrow current profile. The half width for the total driven current is about 10% of the minor radius. The peaked density profile has a more peaked power deposition profile. This will partly offset the effect of trapping and gives rise to a broader maximum, as can be seen in Fig. 5.

4. Conclusions and Discussions

Current to power ratio of the order of 0.45 A/W can be obtained in JET for heating near the fourth harmonic of deuterium cyclotron resonance. Discharges with peaked density and temperature profiles as obtainable with pellet injection have a lower efficiency compared to broad low density profiles with a high electron temperature.

Best efficiency is obtained for intermediate toroidal mode numbers. Trapped particle effect is a severe restriction for current generation by large toroidal numbers. However, it has recently been shown that about half of the current lost by trapped particle effects can be regained via an inverse Ware pinch effect [16].

The main limitation of the current drive efficiency comes from the difficulty of using low toroidal mode numbers. In principle this is an ideal regime for reaching a high efficiency because of the low collisionality, since the wave interaction take place with high energy electrons. The disadvantages with the low toroidal mode numbers comes from the weak TTMP/ELD which makes other absorption processes more important. The approximation of $k_{//}$ by n_ϕ/R for low toroidal mode numbers becomes less relevant. The correction of the parallel wave number for a finite poloidal magnetic field and a finite poloidal wave number becomes important. The absorption will then occur at a higher parallel wave number [14], which will reduce the efficiency.

Acknowledgements.

One of the authors (T. H.) wish to thank the JET theory division for the hospitality shown during his visits. This work has been supported by the European Communities under an association contract between Euratom and Sweden.

References

[1] Ohkawa, T., Nucl. Fusion **10**(1970)185

[2] Wort, D.J.M., Plasma Physics **13**(1971)258

[3] Fish, N.J., Phys. Rev. Lett. **41**(1978)873

[4] Simonen, T.C., Matsuoka, M., Bhadra, D.K., *et al.*, in Plasma Physics and Controlled Nuclear Fusion Research 1988 Proc. 12th Int. Conf. Nice, 1988 / Vol. 1, IAEA, Vienna (1988)669

[5] Hooke, W., Plasma Physics and Controlled Fusion **26**(1984)133

[6] Wong, K.L. and Ono, M., Nucl. Fusion **24**(1984)615

[7] Fish, N.J. and Karney, C.F.F., Phys. Fluids **24**(1981)27; Harvey, R.W., Marx, K.D., McCoy, M.G., Nucl. Fusion **21**(1981)153

[8] Chiu, S.C., Chan, V.S., Harvey, R.W., and Porkolab, M. Nucl. Fusion **29**(1989)2175

[9] Eriksson, L-G., and Hellsten, T., Nucl. Fusion **6**(1989)875

[10] Start, D.F.H., Barlett, D.V., Bhatnagar, V.P., Campbell, P.J., et al submitted to Nucl. Fusion Letters.

[11] Bickerton, R.J., Comments Plasma Physics. Controlled Fusion **1**(1972)95

[12] Porkolab, M., Phys. Fluids **20**(1977)2058

[13] Villard, L., Appert, K., Gruber, R., and Vaclavik, J.,Computer Phys. Reports **4**(1986)95

[14] Llobbet, X., Hellsten, T., and Villard, L. Proc. Joint Varenna-Lausanne Int. Workshop on "Theory of Fusion Plasmas", Chexbres, (1988)

[15] Stix, T. , Nucl. Fusion **15**(1975)737

[16] Elfimov, A.G. and Puri, S., Nucl. Fusion **30**(1990)1215

APPENDIX 1.

THE JET TEAM

JET Joint Undertaking, Abingdon, Oxon, OX14 3EA, U.K.

J.M.Adams[1], F.Alladio[4], H.Altmann, R.J.Anderson, G.Appruzzese, W.Bailey, B.Balet, D.V.Bartlett, L.R.Baylor[24], K.Behringer, A.C.Bell, P.Bertoldi, E.Bertolini, V.Bhatnagar, R.J.Bickerton, A.Boileau[3], T.Bonicelli, S.J.Booth, G.Bosia, M.Botman, D.Boyd[31], H.Brelen, H.Brinkschulte, M.Brusati, T.Budd, M.Bures, T.Businaro[4], H.Buttgereit, D.Cacaut, C.Caldwell-Nichols, D.J.Campbell, P.Card, J.Carwardine, G.Celentano, P.Chabert[27], C.D.Challis, A.Cheetham, J.Christiansen, C.Christodoulopoulos, P.Chuilon, R.Claesen, S.Clement[30], J.P.Coad, P.Colestock[6], S.Conroy[13], M.Cooke, S.Cooper, J.G.Cordey, W.Core, S.Corti, A.E.Costley, G.Cottrell, M.Cox[7], P.Cripwell[13], F.Crisanti[4], D.Cross, H.de Blank[16], J.de Haas[16], L.de Kock, E.Deksnis, G.B.Denne, G.Deschamps, G.Devillars, K.J.Dietz, J.Dobbing, S.E.Dorling, P.G.Doyle, D.F.Düchs, H.Duquenoy, A.Edwards, J.Ehrenberg[14], T.Elevant[12], W.Engelhardt, S.K.Erents[7], L.G.Eriksonn[5], M.Evrard[2], H.Falter, D.Flory, M.Forrest[7], C.Froger, K.Fullard, M.Gadeberg[11], A.Galetsas, R.Galvao[8], A.Gibson, R.D.Gill, A.Gondhalekar, C.Gordon, G.Gorini, C.Gormezano, N.A.Gottardi, C.Gowers, B.J.Green, F.S.Griph, M.Gryzinski[26], R.Haange, G.Hammett[6], W.Han[9], C.J.Hancock, P.J.Harbour, N.C.Hawkes[7], P.Haynes[7], T.Hellsten, J.L.Hemmerich, R.Hemsworth, R.F.Herzog, K.Hirsch[14], J.Hoekzema, W.A.Houlberg[24], J.How, M.Huart, A.Hubbard, T.P.Hughes[32], M.Hugon, M.Huguet, J.Jacquinot, O.N.Jarvis, T.C.Jernigan[24], E.Joffrin, E.M.Jones, L.P.D.F.Jones, T.T.C.Jones, J.Källne, A.Kaye, B.E.Keen, M.Keilhacker, G.J.Kelly, A.Khare[15], S.Knowlton, A.Konstantellos, M.Kovanen[21], P.Kupschus, P.Lallia, J.R.Last, L.Lauro-Taroni, M.Laux[33], K.Lawson[7], E.Lazzaro, M.Lennholm, X.Litaudon, P.Lomas, M.Lorentz-Gottardi[2], C.Lowry, G.Magyar, D.Maisonnier, M.Malacarne, V.Marchese, P.Massmann, L.McCarthy[28], G.McCracken[7], P.Mendonca, P.Meriguet, P.Micozzi[4], S.F.Mills, P.Millward, S.L.Milora[24], A.Moissonnier, P.L.Mondino, D.Moreau[17], P.Morgan, H.Morsi[14], G.Murphy, M.F.Nave, M.Newman, L.Nickesson, P.Nielsen, P.Noll, W.Obert, D.O'Brien, J.O'Rourke, M.G.Pacco-Düchs, M.Pain, S.Papastergiou, D.Pasini[20], M.Paume[27], N.Peacock[7], D.Pearson[13], F.Pegoraro, M.Pick, S.Pitcher[7], J.Plancoulaine, J-P.Poffé, F.Porcelli, R.Prentice, T.Raimondi, J.Ramette[17], J.M.Rax[27], C.Raymond, P-H.Rebut, J.Removille, F.Rimini, D.Robinson[7], A.Rolfe, R.T.Ross, L.Rossi, G.Rupprecht[14], R.Rushton, P.Rutter, H.C.Sack, G.Sadler, N.Salmon[13], H.Salzmann[14], A.Santagiustina, D.Schissel[25], P.H.Schild, M.Schmid, G.Schmidt[6], R.L.Shaw, A.Sibley, R.Simonini, J.Sips[16], P.Smeulders, J.Snipes, S.Sommers, L.Sonnerup, K.Sonnenberg, M.Stamp, P.Stangeby[19], D.Start, C.A.Steed, D.Stork, P.E.Stott, T.E.Stringer, D.Stubberfield, T.Sugie[18], D.Summers, H.Summers[20], J.Taboda-Duarte[22], J.Tagle[30], H.Tamnen, A.Tanga, A.Taroni, C.Tebaldi[23], A.Tesini, P.R.Thomas, E.Thompson, K.Thomsen[11], P.Trevalion, M.Tschudin, B.Tubbing, K.Uchino[29], E.Usselmann, H.van der Beken, M.von Hellermann, T.Wade, C.Walker, B.A.Wallander, M.Walravens, K.Walter, D.Ward, M.L.Watkins, J.Wesson, D.H.Wheeler, J.Wilks, U.Willen[12], D.Wilson, T.Winkel, C.Woodward, M.Wykes, I.D.Young, L.Zannelli, M.Zarnstorff[6], D.Zasche[14], J.W.Zwart.

PERMANENT ADDRESS

1. UKAEA, Harwell, Oxon. UK.
2. EUR-EB Association, LPP-ERM/KMS, B-1040 Brussels, Belgium.
3. Institute National des Récherches Scientifique, Quebec, Canada.
4. ENEA-CENTRO Di Frascati, I-00044 Frascati, Roma, Italy.
5. Chalmers University of Technology, Göteborg, Sweden.
6. Princeton Plasma Physics Laboratory, New Jersey, USA.
7. UKAEA Culham Laboratory, Abingdon, Oxon. UK.
8. Plasma Physics Laboratory, Space Research Institute, Sao José dos Campos, Brazil.
9. Institute of Mathematics, University of Oxford, UK.
10. CRPP/EPFL, 21 Avenue des Bains, CH-1007 Lausanne, Switzerland.
11. Risø National Laboratory, DK-4000 Roskilde, Denmark.
12. Swedish Energy Research Commission, S-10072 Stockholm, Sweden.
13. Imperial College of Science and Technology, University of London, UK.
14. Max Planck Institut für Plasmaphysik, D-8046 Garching bei München, FRG.
15. Institute for Plasma Research, Gandhinagar Bhat Gujat, India.
16. FOM Instituut voor Plasmafysica, 3430 Be Nieuwegein, The Netherlands.
17. Commissiariat à L'Energie Atomique, F-92260 Fontenay-aux-Roses, France.
18. JAERI, Tokai Research Establishment, Tokai-Mura, Naka-Gun, Japan.
19. Institute for Aerospace Studies, University of Toronto, Downsview, Ontario, Canada.
20. University of Strathclyde, Glasgow, G4 ONG, U.K.
21. Nuclear Engineering Laboratory, Lapeenranta University, Finland.
22. JNICT, Lisboa, Portugal.
23. Department of Mathematics, Univeristy of Bologna, Italy.
24. Oak Ridge National Laboratory, Oak Ridge, Tenn., USA.
25. G.A. Technologies, San Diego, California, USA.
26. Institute for Nuclear Studies, Swierk, Poland.
27. Commissiariat à l'Energie Atomique, Cadarache, France.
28. School of Physical Sciences, Flinders University of South Australia, South Australia SO42.
29. Kyushi University, Kasagu Fukuoka, Japan.
30. Centro de Investigaciones Energeticas Medioambientales y Techalogicas, Spain.
31. University of Maryland, College Park, Maryland, USA.
32. University of Essex, Colchester, UK.
33. Akademie de Wissenschaften, Berlin, DDR.

CR 88.49.1A